Rapid Communications

Critical excitation-inhibition balance in dense neural networks

Lorenz Baumgarten* and Stefan Bornholdt†
Institut für Theoretische Physik, Universität Bremen, 28759 Bremen, Germany

(Received 29 March 2019; published 10 July 2019)

The "edge of chaos" phase transition in artificial neural networks is of renewed interest in light of recent evidence for criticality in brain dynamics. Statistical mechanics traditionally studied this transition with connectivity k as the control parameter and an exactly balanced excitation-inhibition ratio. While critical connectivity has been found to be low in these model systems, typically around $k = 2$, which is unrealistic for natural neural systems, a recent study utilizing the excitation-inhibition ratio as the control parameter found a new, nearly degree independent, critical point when connectivity is large. However, the new phase transition is accompanied by an unnaturally high level of activity in the network. Here we study random neural networks with the additional properties of (i) a high clustering coefficient and (ii) neurons that are solely either excitatory or inhibitory, a prominent property of natural neurons. As a result, we observe an additional critical point for networks with large connectivity, regardless of degree distribution, which exhibits low activity levels that compare well with neuronal brain networks.

DOI: 10.1103/PhysRevE.100.010301

Between the ordered and chaotic regimes of threshold neural networks lies the "edge of chaos," a critical point where the length and size distributions of activity avalanches are governed by characteristic power laws. This dynamical phase transition has been thoroughly studied in random neural networks [1–4], nonsymmetric spin glasses [5], and random Boolean networks [6–10]. Traditionally, threshold neural networks have been studied with precisely balanced excitation and inhibition, usually by randomly assigning activating and inhibiting links with equal probabilities. In these networks, criticality occurs for small average degrees k [1]. However, when allowing the fraction of excitatory links F_+ as a second control parameter of the phase transition, it was recently discovered that there exist two critical lines in the k-F_+-plane: one almost parallel to the F_+ axis at low k and one almost independent of k at some $F_+ > 0.5$ [11]; see Fig. 1.

The relevance of this new critical point becomes apparent in the context of neural brain networks which exhibit a high average degree ($k \approx 10^4$ in human brains [12]) and a characteristic imbalance between excitation and inhibition (20–30% of neurons are inhibitory in monkey brains [13]). There is a large amount of evidence suggesting that the brain operates near a critical point, namely, avalanche sizes and durations governed by power laws [14–19], the possibility of tuning from a subcritical regime through the critical point to a supercritical regime [20], mathematical relations between critical exponents, and collapsible avalanche shapes [15,19,21]. Further, Fraiman *et al.* showed striking similarities between correlation networks extracted from brains and the Ising model at the critical point [22]. The interest in the role of criticality in the brain is illustrated by the large amount of research devoted to criticality in network models inspired by biological networks [23–30].

Unfortunately, the high-degree critical point of Fig. 1 exists in a high-activity regime which is unrealistic for brain networks. We find, however, an additional critical point that persists at low activities, at the left flank of the high sensitivity region, when including additional network properties characteristic of brain networks, thereby providing a more likely network model candidate for describing the processes behind brain criticality.

We use threshold networks consisting of N nodes connected by kN directed edges, whose node states are updated in parallel according to

$$\sigma_i(t+1) = \begin{cases} 1 & \text{if } \sum_{j=1}^{N} w_{ij}\sigma_j(t) > h \\ 0 & \text{if } \sum_{j=1}^{N} w_{ij}\sigma_j(t) \leqslant h, \end{cases} \tag{1}$$

where $\sigma_i(t)$ is the node i's state at time t and w_{ij} is the weight of the connection from node j to node i. The weights w_{ij} can be 0 if there is no connection between nodes i and j, or ± 1 otherwise. The weights of existing connections are chosen randomly with excitatory links $w_{ij} = +1$ chosen with probability F_+. Initial states of the nodes are chosen according to a random initial activity $A_0 = \frac{1}{N}\sum_i \sigma_i$.

A simple quantity that we use to measure criticality is the sensitivity λ [31,32]. Imagine switching one node's state in the current time step; then λ is defined as the average number of nodes whose states will then be different in the next time step from what they would have been otherwise. If sensitivity is smaller or larger than 1, perturbations will quickly die out or dominate the entire network, respectively. Hence, at $\lambda = 1$, the network is in a critical state.

First, in order to establish whether the vertical white line defined by $\lambda = 1$ seen in Fig. 1 indeed is a critical point, we measure the averages of multiple quantities of interest, as well as the average sensitivity for 10^3 time steps after letting the network relax from its initial condition within 2×10^3 time steps (tests show that increasing this time or waiting until an attractor is reached—where possible, attractors cannot be

*lbaumgarten@itp.uni-bremen.de
†bornholdt@itp.uni-bremen.de

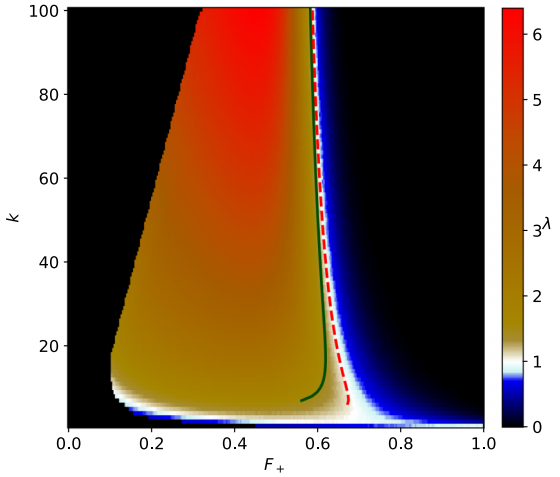

FIG. 1. Sensitivity as a function of fraction of excitatory links F_+ and connectivity k in random neural networks, similar to Fig. 1C in [11], for threshold $h = 0$ and $N = 10^3$ nodes. Lines compare Eq. (3) (green solid line) and the numerical solution of Eq. (2) (red dashed line) with the simulation results. Both lines approximate the simulation's critical line well for large k. Note that the left flank of the sensitive region of the simulation does not exhibit a (white) critical corridor, which is further discussed in the text.

found in a reasonable amount of time for $\lambda \gg 1$—does not change the results) for different values of F_+. Afterwards, we can plot the measured quantities as a function of sensitivity. The measured quantities are the network's activity A, the fraction of nodes which do not change their state within the 10^3 time steps N_S, and the average number of state changes per node and time step F/Nt. This measurement is shown in Fig. 2.

For $\lambda < 1$, essentially all nodes are static (i.e., remaining in one state, either active or inactive) and almost no flips happen, whereas for $\lambda > 1$, the number of static nodes drops and the number of flips increases, so $\lambda = 1$ is a boundary between order and chaos. Also note that the network's activity is very high at the critical point. It seems, therefore, that this critical point cannot underlie a mechanism that defines criticality in the brain, as almost all neurons constantly firing is not realistic.

Further, we measure avalanche sizes and durations at the critical point, as described in the Supplemental Material [33]; see Fig. 3. We observe power laws in both avalanche size and duration distributions.

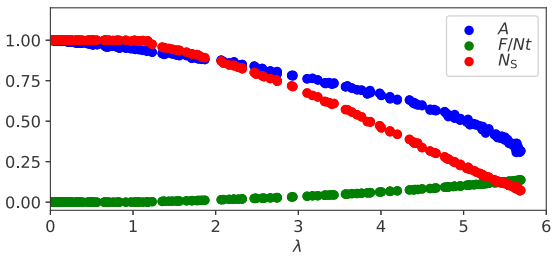

FIG. 2. Activity A, static node fraction N_S, and flips per node and time step F/Nt as a function of the sensitivity λ for $k = 80$, $N = 10^4$, and $h = 1$.

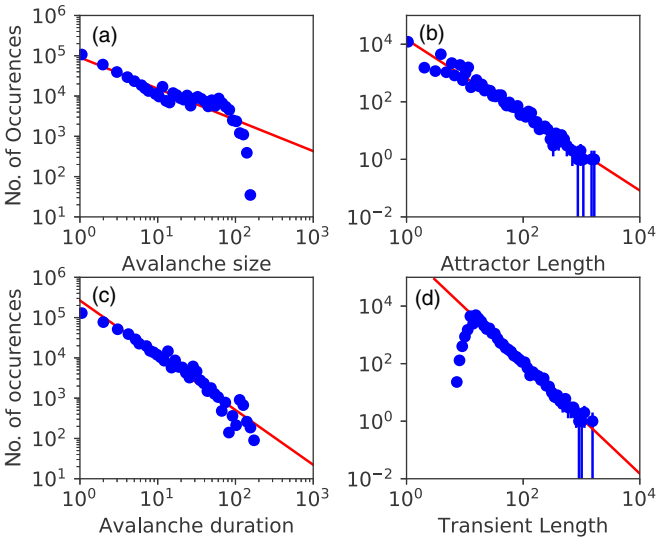

FIG. 3. Distributions of avalanches. (a) Sizes and (c) durations for networks with $F_+ \approx 0.6$, $k = 80$, $N = 10^4$, and $h = 1$. The slopes shown in red are (a) -0.8 and (c) -1.4. Also, (b) attractor and (d) transient length distributions for networks with $0.95 \leqslant \lambda \leqslant 1.05$, $F_+ \approx 0.6$, $k = 80$, $N = 4444$, and $h = 1$. The slopes shown in red are (b) -1.3 and (d) -1.9. Logarithmic binning is used for all four figures.

Finally, we measure the attractor and transient lengths, as well as the average sensitivity within the attractor for a number of different network realizations for fixed parameters. We only use parameter and attractor lengths of networks whose average sensitivity λ is within $1 - \delta \leqslant \lambda \leqslant 1 + \delta$ with $\delta = 0.05$. Attractor and transient length distributions are shown in Fig. 3. Both the attractor lengths as well as the right flank of the transient length distributions show clear power laws, as is to be expected for critical networks [34].

All of the above discussed properties lead us to conclude that this is indeed a critical point.

We use Derrida's annealed approximation [6], adopted for threshold networks [2], to estimate the critical F_+ as a function of k, and arrive at the equation

$$\frac{1}{k} = \binom{k}{\frac{k+h+1}{2}} F_+^{\frac{k+h+1}{2}} (1 - F_+)^{\frac{k-h-1}{2}} \frac{k+h+1}{2k}. \tag{2}$$

Under the assumption of large average degree $k \gg h$, $k \gg 1$, this can be simplified to

$$F_+ = \frac{1}{2}\left[1 + \left\{1 - \left(\frac{2\pi}{k}\right)^{\frac{k}{2}}\right\}^{\frac{1}{2}}\right]. \tag{3}$$

See the Supplemental Material [33] for details. Figure 1 shows a comparison of Eq. (3), as well as the numerical solution of Eq. (2), with our simulation results.

Let us now focus on the the left flank of the central high sensitivity region in Fig. 1. When lowering the value of F_+ from intermediate values towards 0, sensitivity λ seems to suddenly drop to 0 from values larger than 1. In the simulations, this is due to a sudden drop in persistent activity: All activity dies out before the average sensitivity crosses through one. Critical sensitivity here falls into the left (black) region

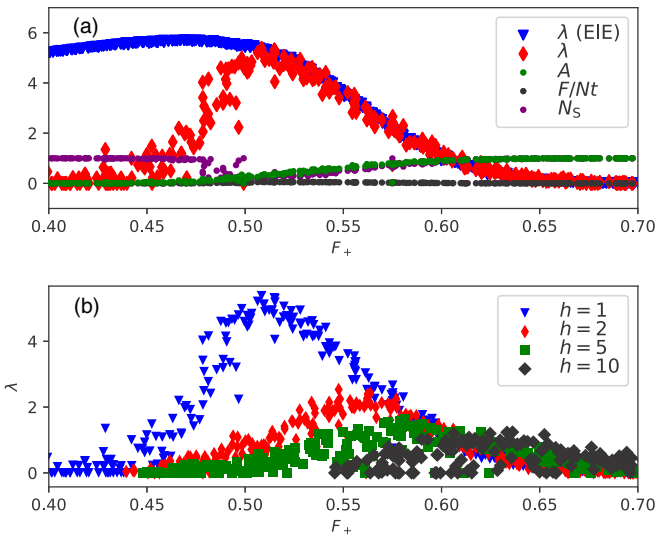

FIG. 4. (a) Activity A, static node fraction N_S, flips per node and time step F/Nt, and sensitivity λ at $h = 1$ and (b) sensitivity λ for different thresholds h as a function of F_+ for $k = 80$, $N = 10^4$, and WS-EIN networks with rewiring probability $\beta = 10^{-2}$ ($C \approx 0.72$). The sensitivity for an equivalent ER network ($C = 0.008$) is also shown in (a) for comparison.

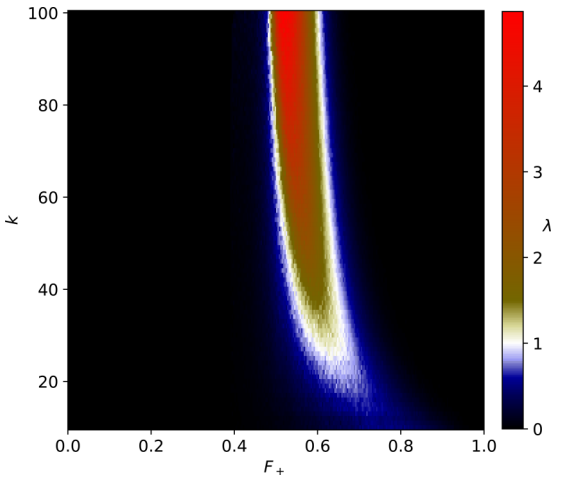

FIG. 5. Sensitivity as a function of fraction of excitatory links F_+ and connectivity k in clustered EIN (Dale) neural networks for threshold $h = 2$, clustering coefficient $C = 0.65$, and $N = 10^4$ nodes.

of entirely inactive networks, whose sensitivity is not shown (as only persisting activity is relevant and, therefore, plotted).

However, as a central observation of our study, we find that networks can be kept from abruptly dying out for low F_+ by introducing two properties to the network: increasing the networks' clustering coefficient C and requiring that nodes have either only excitatory or only inhibitory outgoing edges (Dale's principle). Both of these properties are prominent features of brain networks [35–39]. Note that these properties do not necessarily cause networks to show finite activity for values of F_+ in which the random network has zero activity, but instead that the activity goes continuously towards zero with lowering F_+ instead of abruptly dropping to zero.

We believe the mechanism underlying the left flank's survival to be as follows: If two excitatory nodes which are connected to each other are active, then for high clustering coefficients, they are likely to have shared neighbors and can therefore combine their efforts to also activate these neighbors more easily than in random networks and thereby create islands of surviving activity. The contribution of nodes being either excitatory or inhibitory is likely that if few random nodes are active within a region, this property significantly increases the variance of the relative number of activating signals in that region and therefore increases the probability of areas exhibiting high excitation by random chance.

We also see that the sensitivity in clustered graphs with nodes either fully excitatory or inhibitory closely follows the sensitivity of random graphs for high values of F_+, but then drops off for lower F_+; see Fig. 4. This is likely due to nodes in the center of activity islands receiving many more excitatory connections than necessary for activation. This both lowers the overall activity because these redundant excitatory signals essentially lower the network's total excitation and lowers the sensitivity because only nodes with an input sum near the excitation threshold contribute to it.

Networks with only a high clustering coefficient, without the second property of nodes having either only excitatory or only inhibitory outgoing edges, can also show surviving activity on the left flank for some initial configurations and for exceedingly high clustering coefficients and thresholds, but even then the left flank drops sharply towards zero. In the following, let us denote networks obeying Dale's principle [39], i.e., networks consisting of excitatory neurons and inhibitory neurons as *EIN networks*, as opposed to networks with excitatory-inhibitory edges which we will call *EIE networks*.

Since the network's activity does not abruptly die out on the left flank anymore for clustered EIN networks, a second critical point can be found here, as shown in Fig. 5 and Fig. 4(a). Plotting the sensitivity in the F_+-k plane in Fig. 5, we now see that the left flank indeed exhibits critical sensitivity $\lambda = 1$ (white color). Note that in contrast to the first critical point at the right flank of the sensitive region, this second critical point at the left flank exists in a low-activity state, making it more interesting for real-life applications, such as studying mechanisms underlying brain criticality.

To construct networks with different high clustering coefficients, here we use directed Watts-Strogatz (WS) networks [40,41]. The original WS model consists of a ring of N neurons with periodic boundary conditions in which every neuron is connected to its k nearest neighbors. Then, connections are randomly rewired with rewiring probability β. We use an essentially equivalent implementation without explicit rewiring from [41] in which the probability of a connection from a node i to a node j existing is

$$\begin{aligned} p_{ij} = {} & \beta p_0 + (1-\beta)\Theta[p_0 - D_{ij}/(N/2)] \\ & + \tfrac{1}{2}(1-\beta)\Theta[p_0 + D_{ij}/(N/2)] \\ & \times \Theta[p_0 - (D_{ij} - 0.5)/(N/2)], \end{aligned} \tag{4}$$

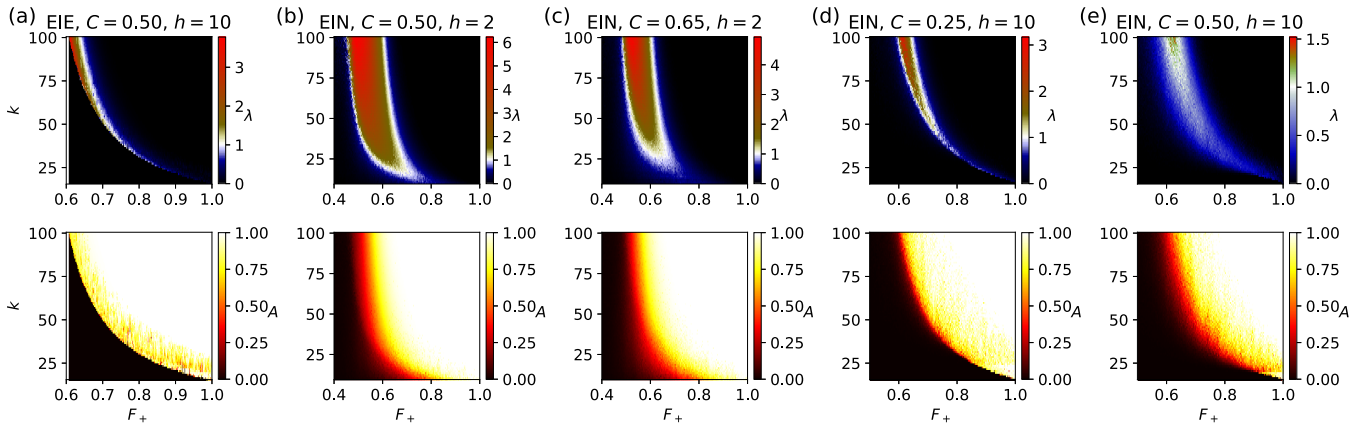

FIG. 6. Sensitivity λ and activity A for different network configurations. White denotes a critical sensitivity. (a) For EIE networks—except for very high clustering coefficients and thresholds—the left flank dies out before reaching the critical point. (b) Switching to an EIN network stabilizes the left flank; however, it still collapses for high average degrees k without a high clustering coefficient. Some white artifacts can be seen because the left flank does not die out within 2×10^3 time steps; it does, however, die out after a larger number of time steps, and therefore no second critical point exists here; see Supplemental Material [33] for more information. (c) A higher clustering coefficient $C = 0.65$ stabilizes the left flank even for higher average degrees k (this case is taken from Fig. 5). (d) With a higher threshold $h = 10$, even a lower clustering coefficient $C = 0.25$ can have a stable left flank. The distance between the critical points shrinks for higher thresholds and both critical points are also moved to higher F_+. (e) For EIN networks, a higher clustering coefficient ($C = 0.5$) lowers the network's average sensitivity, leading this configuration to only barely pass above $\lambda = 1$ between the critical points. From the shape of the left critical line from (b) to (d), it can also be seen that the left critical line is merely a continuation of the horizontal line from Fig. 1 folded upwards.

where $p_0 = k/(N-1)$ and D_{ij} is the distance between nodes i and j on the ring, i.e., $D_{ij} = \min(|i-j|, N-|i-j|)$. The third term has been added to enable uneven values of k. By manipulating the rewiring probability β, we can vary a network's clustering coefficient and average path length. The Watts-Strogatz model's strength is that when varying β, there is a region in which the clustering coefficient is nearly constant while the average path length changes drastically and a second region in which the clustering coefficient changes and the average path length is nearly constant, enabling us to isolate these two parameters' effects.

In our study of clustered EIN networks, we find that the second critical point comes into existence in the region in which the clustering coefficient changes, while it is unaffected by changes within the region in which the clustering coefficient is constant. Therefore, a high clustering coefficient is sufficient to enable the second critical point's existence.

The influence of thresholds and clustering coefficients, as well as the difference between EIE and EIN networks is shown in Figs. 4(b) and 6.

So far, our networks had degree distributions centered around an average value; however, random or Watts-Strogatz models rarely describe real-life networks. Scale-free or similar networks with a broad degree distribution are significantly more abundant in nature. In fact, for neuronal networks, cumulative degree distributions ranging from power laws [42–44] over exponentially truncated power laws [45–49] to exponential laws [50–53] have been found, with the observation that distributions following exponentially truncated power laws increasingly resemble true power laws for measurements on finer scales [45].

In analogy to the brain, we focus on EIN networks with a broad link distribution. For generating the topology, we require an algorithm that (1) can produce a scale-free graph in which low-degree nodes can exist, (2) can initialize large networks fast, (3) can produce networks with variable clustering coefficient, as we have already seen that this can have a large impact on criticality, and, if possible, (4) can also produce other degree distributions similar to scale-free graphs.

For this purpose, we adapt the algorithm described by Lo *et al.* [54], a particularly efficient implementation of preferential attachment [55], to fit our criteria.

In our algorithm, we start with a single node and iteratively add a connection between two nodes every two time steps, so that the sum of in and out degrees in the network increases by one per time step. The origins and targets of these added nodes are chosen by preferential attachment, meaning that the probability of a node being chosen is proportional to the sum of its in and out degree plus an offset δ, which ensures that the probability of previously unconnected nodes receiving connections is nonzero. Further, every m time steps, a new node is added to the network. One significant difference between our algorithm and other algorithms creating scale-free graphs is that the newly added edges need not connect to the newly added node, but can instead connect any two nodes in the system, allowing low-degree nodes to exist in the final network.

This process is repeated multiple times and the connections of every initialization are added together into one network until the desired average degree is reached. Finally, we add i random incoming and outgoing connections to every node, where i is the first integer with $i > h$, so that all nodes have the chance of being activated. For a detailed description of this algorithm, see the Supplemental Material [33].

The two parameters δ and m control whether the resulting degree distribution is scale free or an exponentially truncated power law and also the clustering coefficient. In general,

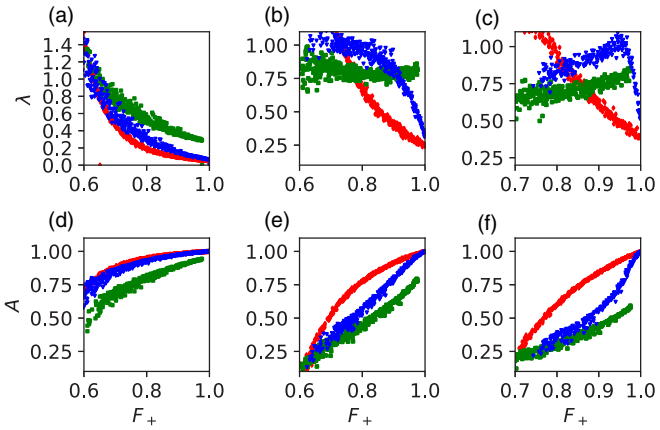

FIG. 7. (a)–(c) Sensitivity λ and (d)–(f) activity A as a function of F_+ for an exponentially truncated power law network with low clustering coefficient ($\delta = 40, m = 2$) (red) and a scale-free network with high clustering coefficient, where the largest node is excitatory ($\delta = 1, m = 10$) (green) or inhibitory (blue) at $k = 40$, $N = 10^4$, and (a), (d) $h = 1$, (b), (e) $h = 7$, (c), (f) $h = 10$. The sensitivity and activity for the highly clustered network were measured as the average within the network's attractor.

lower δ and higher m lead to scale-free distributions with high clustering, whereas high δ and low m lead to low clustering truncated power law distributions.

Studying the dynamics of EIN networks with such a topology, we find that for scale-free graphs, the right critical point still exists (see Fig. 7), and that the sensitivity λ splits into two paths on the right flank and is therefore no longer solely dependent on F_+. The two different paths are dependent on whether the network's largest node is excitatory or inhibitory (in our algorithm, there is a clear hierarchy between nodes, dictated by when they were introduced to the network, and therefore the first node is always clearly larger than the rest, so no multiple nodes are competing for the spot of largest node). Similarly to the existence of the left flank in WS networks, this split in the sensitivity is amplified by high clustering coefficients and thresholds.

Figure 7 also shows the existence of the left flank's second critical point for high clustering coefficients C and thresholds h; see Fig. 7. For low clustering coefficients, the left flank still dies out. High clustering coefficients and thresholds lower the sensitivity curve's slope, so that for certain parameters, the sensitivity, and therefore criticality, is almost constant over a wide area of F_+; see Fig. 7(b).

To summarize, in threshold neural networks, a phase transition between a chaotic and a quiescent regime has been found for highly clustered networks with exclusively excitatory-inhibitory nodes. This critical point exhibits a persisting, yet low level of average activity (which in unclustered networks would die out). Besides the requirement of a certain level of clustering, it is robust both for random as well as broad (scale-free) degree distributions.

This new critical point is of particular interest to neuroscience because it is relatively independent of the degree k and may, therefore, occur at the large average degree present in brains. Furthermore, the main prerequisites for this critical point's existence are present in the brain: a highly clustered architecture and nodes being either exclusively excitatory or inhibitory (Dale's principle).

It can only be speculated what role criticality may play in nature. It has been discussed that it could optimize a network's information processing capabilities. Yet also, dynamical phase transitions are a simple means that physics provides, allowing a complex system to tune to an intermediate activity regime with great ease.

Last, but not least, research has shown that the balance between excitation and inhibition in the brain, which needs to be a specific value for a network to be critical in our model, is vital for a functioning brain [56–60] and that disturbing this balance can negatively impact information processing [61]. Interestingly, the ratio of excitatory and inhibitory neurons in brain networks is observed to be almost constant throughout an organism's development, and feedback algorithms that regulate this ratio are currently discussed [62]. This supports our hypothesis that the critical point described in this Rapid Communication, resulting from the statistical mechanics of a dynamical phase transition, may provide a natural target value for mechanisms that regulate the excitation-inhibition balance in the brain.

[1] K. Kürten, Phys. Lett. A **129**, 157 (1988).
[2] S. Bornholdt and T. Rohlf, Physica A **310**, 245 (2002).
[3] A. Szejka, T. Mihaljev, and B. Drossel, New J. Phys. **10**, 063009 (2008).
[4] T. Rohlf, Phys. Rev. E **78**, 066118 (2008).
[5] B. Derrida, J. Phys. A **20**, L721 (1987).
[6] B. Derrida and Y. Pomeau, Europhys. Lett. **1**, 45 (1986).
[7] K. E. Kürten, J. Phys. A **21**, L615 (1988).
[8] M. Aldana, S. Coppersmith, and L. Kadanoff, in *Perspectives and Problems in Nolinear Science*, edited by E. Kaplan, J. Marsden, and K. Sreenivasan (Springer, New York, 2003).
[9] B. Drossel, in *Reviews of Nonlinear Dynamics and Complexity*, Vol. 1, edited by H. Schuster (Wiley-VCH, Weinheim, 2008).
[10] S. Bornholdt and S. Kauffman, J. Theor. Biol. **467**, 15 (2019).
[11] J. Neto, M. de Aguiar, J. Brum, and S. Bornholdt, arXiv:1712.08816.
[12] P. R. Huttenlocher, Brain Res. **163**, 195 (1979).
[13] S. Hendry, H. D. Schwark, E. Jones, and J. Yan, J. Neurosci. **7**, 1503 (1987).
[14] J. Beggs and D. Plenz, J. Neurosci. **23**, 11167 (2003).
[15] N. Friedman, S. Ito, B. A. W. Brinkman, M. Shimono, R. E. Lee DeVille, K. A. Dahmen, J. M. Beggs, and T. C. Butler, Phys. Rev. Lett. **108**, 208102 (2012).
[16] V. Priesemann, M. Wibral, M. Valderrama, R. Pröpper, M. Quyen, T. Geisel, J. Triesch, D. Nikolić, and M. Munk, Front. Syst. Neurosci. **8**, 108 (2014).
[17] N. Timme, N. Marshall, N. Bennett, M. Ripp, E. Lautzenhiser, and J. Beggs, Front. Physiol. **7**, 425 (2016).

[18] M. Yaghoubi, T. de Graaf, J. Orlandi, F. Girotto, M. Colicos, and J. Davidsen, Sci. Rep. **8**, 3417 (2018).
[19] A. J. Fontenele, N. A. P. de Vasconcelos, T. Feliciano, L. A. A. Aguiar, C. Soares-Cunha, B. Coimbra, L. Dalla Porta, S. Ribeiro, A. J. Rodrigues, N. Sousa, P. V. Carelli, and M. Copelli, Phys. Rev. Lett. **122**, 208101 (2019).
[20] C. Haldeman and J. M. Beggs, Phys. Rev. Lett. **94**, 058101 (2005).
[21] A. Shaukat and J. Thivierge, Front. Comput. Neurosci. **10**, 29 (2016).
[22] D. Fraiman, P. Balenzuela, J. Foss, and D. R. Chialvo, Phys. Rev. E **79**, 061922 (2009).
[23] T. Gross and B. Blasius, J. R. Soc. Interface **5**, 259 (2007).
[24] X. Li, Q. Chen, and F. Xue, Phil. Trans. R. Soc. A **375**, 20160286 (2017).
[25] W. Clawson, N. Wright, R. Wessel, and W. Shew, PLoS Comput. Biol. **13**, e1005574 (2017).
[26] L. Brochini, A. de Andrade Costa, M. Abadi, A. Roque, J. Stolfi, and O. Kinouchi, Sci. Rep. **6**, 35831 (2016).
[27] S. Gautam, T. Hoang, K. McClanahan, S. Grady, and W. Shew, PLoS Comput. Biol. **11**, e1004576 (2015).
[28] O. Shriki and D. Yellin, PLoS Comput. Biol. **12**, e1004698 (2016).
[29] B. V. Rodriguez, A. Avena-Koenigsberger, O. Sporns, A. Griffa, P. Hagmann, and H. Larralde, Sci. Rep. **7**, 13020 (2017).
[30] M. Ferraz, H. Melo-Silva, and A. Kihara, PLoS One **12**, e0184367 (2017).
[31] B. Luque and R. V. Solé, Phys. Rev. E **55**, 257 (1997).
[32] I. Shmulevich and S. A. Kauffman, Phys. Rev. Lett. **93**, 048701 (2004).
[33] See Supplemental Material at http://link.aps.org/supplemental/10.1103/PhysRevE.100.010301 for details on the annealed approximation and simulation methods.
[34] A. Bhattacharjya and S. Liang, Phys. Rev. Lett. **77**, 1644 (1996).
[35] K. E. Stephan, C.-C. Hilgetag, G. A. P. C. Burns, M. A. O'Neill, M. P. Young, and R. Kötter, Philos. Trans. R. Soc. London B Biol. Sci. **355**, 111 (2000).
[36] O. Sporns and J. D. Zwi, Neuroinformat. **2**, 145 (2004).
[37] O. Sporns, C. J. Honey, and R. Kötter, PLoS One **2**, e1049 (2007).
[38] D. S. Bassett and E. Bullmore, Neuroscientist **12**, 512 (2006).
[39] H. Dale, Proc. R. Soc. Med. **28**, 319 (1935).
[40] D. Watts and S. Strogatz, Nature(London) **393**, 440 (1998).
[41] H. F. Song and X.-J. Wang, Phys. Rev. E **90**, 062801 (2014).
[42] L. Varshney, B. Chen, E. Paniagua, D. Hall, and D. Chklovskii, PLoS Comput. Biol. **7**, e1001066 (2011).
[43] M. van den Heuvel, C. Stam, M. Boersma, and H. H. Pol, Neuroimage **43**, 528 (2008).
[44] V. Eguíluz, D. Chialvo, G. Cecchi, M. Baliki, and A. Apkarian, Phys. Rev. Lett. **94**, 018102 (2005).
[45] S. Hayasaka and P. Laurienti, Neuroimage **50**, 499 (2010).
[46] Y. He, Z. Chen, and A. Evans, Cereb. Cortex **17**, 2407 (2007).
[47] Y. Iturria-Medina, R. Sotero, E. Canales-Rodríguez, Y. Alemán-Gómez, and L. Melia-Garcia, Neuroimage **40**, 1064 (2008).
[48] S. Achard, R. Salvador, B. Whitcher, J. Suckling, and E. Bullmore, Neurosci. **26**, 63 (2006).
[49] G. Gong, Y. He, L. Concha, C. Lebel, D. Gross, A. Evans, and C. Beaulieu, Cereb. Cortex **19**, 524 (2009).
[50] D. Modha and R. Singh, Proc. Natl. Acad. Sci. USA **107**, 13485 (2010).
[51] L. Amaral, A. Scala, M. Barthélémy, and H. Stanley, Proc. Natl. Acad. Sci. USA **97**, 11149 (2000).
[52] P. Hagmann, L. Cammoun, X. Gagandet, R. Meuli, C. Honey, V. Wedeen, and O. Sporns, PLoS Biol. **6**, e159 (2008).
[53] D. de Santos-Sierra, I. Sendiña-Nadal, I. Leyva, J. A. Almendral, S. Anava, A. Ayali, D. Papo, and S. Boccaletti, PloS One **9**, e85828 (2014).
[54] Y. C. Lo, C. T. Li, and S. D. Lin, *International Conference on Privacy, Security, Risk and Trust and International Conference on Social Computing, SocialCom-PASSAT 28* (IEEE, Piscataway, NJ, 2012), pp. 229–238.
[55] A. Barabási and R. Albert, Science **286**, 509 (1999).
[56] B. Haider, A. Duque, A. R. Hasenstaub, and D. A. McCormick, J. Neurosci. **26**, 4535 (2006).
[57] J. L. R. Rubenstein and M. M. Merzenich, Genes Brain Behav. **2**, 255 (2003).
[58] E. C. Davenport, B. R. Szulc, J. Drew, J. Taylor, T. Morgan, N. F. Higgs, G. López-Doménech, and J. T. Kittler, Cell Rep. **26**, 2037 (2019).
[59] M. W. Antoine, T. Langberg, P. Schnepel, and D. E. Feldman, Neuron **101**, 648 (2019).
[60] J. D. Murray and X.-J. Wang, in *Computational Psychiatry*, edited by A. Anticevic and J. D. Murray (Academic Press, Cambridge, MA, 2018), pp. 3–25.
[61] O. Yizhar, L. E. Fenno, M. Prigge, F. Schneider, T. J. Davidson, D. J. O'Shea, V. S. Sohal, I. Goshen, J. Finkelstein, J. T. Paz, K. Stehfest, R. Fudim, C. Ramakrishnan, J. R. Huguenard, P. Hegemann, and K. Deisseroth, Nature (London) **477**, 171 (2011).
[62] S. Sahara, Y. Yanagawa, D. D. M. O'Leary, and C. F. Stevens, J. Neurosci. **32**, 4755 (2012).